

Beneficial influence of Hf and Zr additions to Nb4at.%Ta on the vortex pinning of Nb₃Sn with and without an O source

Shreyas Balachandran^{1*}, Chiara Tarantini¹, Peter J. Lee¹, Fumitake Kametani^{1,2}, Yi-Feng Su¹, Benjamin Walker^{1,2}, William L. Starch¹, and David C. Larbalestier^{1,2}

¹ National High Magnetic Field Laboratory, Tallahassee, FL 32310, USA.

² FAMU/FSU College of Engineering, Tallahassee, FL 32310, USA.

E-mail: shreyasb@asc.magnet.fsu.edu

Abstract

Here we show that addition of Hf to Nb4Ta can significantly improve the high field performance of Nb₃Sn, making it suitable for dipole magnets for a machine like the 100 TeV future circular collider (FCC). A big challenge of the FCC is that the desired non-Cu critical current density (J_c) target of 1500 A/mm² (16 T, 4.2 K) is substantially above the best present Nb₃Sn conductors doped with Ti or Ta (~1300 A/mm² in the very best sample of the very best commercial wire). Recent success with internal oxidation of Nb-Zr precursor has shown significant improvement in the layer J_c of Nb₃Sn wires, albeit with the complication of providing an internal oxygen diffusion pathway and avoiding degradation of the irreversibility field H_{irr} . We here extend the Nb1Zr oxidation approach by comparing Zr and Hf additions to the standard Nb4Ta alloy of maximum H_{c2} and H_{irr} . Nb4Ta rods with 1Zr or 1Hf were made into monofilament wires with and without SnO₂ and their properties measured over the entire superconducting range at fields up to 31 T. We found that group IV alloying of Nb4Ta does raise H_{irr} , though adding O₂ still degrades this slightly. As noted in earlier Nb1Zr work with an O source, the pinning force density F_p is strongly enhanced and its peak value shifted to higher field by internal oxidation. A surprising result of this work is that we found better properties in Nb4Ta1Hf without SnO₂, F_{pMax} achieving 2.35 Times that of the standard Nb4Ta alloy, while the oxidized Nb4Ta1Zr alloy achieved 1.54 times that of the Nb4Ta alloy. The highest layer J_c (16 T, 4.2 K) of 3700 A/mm² was found in the SnO₂-free wire made with Nb4Ta1Hf alloy. Using a standard A15 cross-section fraction of 60% for modern PIT and RRP wires, we estimated that a non-Cu J_c of 2200 A/mm² is obtainable in modern conductors, well above the 1500 A/mm² FCC specification. Moreover, since the best properties were obtained without SnO₂, the Nb4Ta1Hf alloy appears to open a straightforward route to enhanced properties in Nb₃Sn wires manufactured by virtually all the presently used commercial routes employed today.

Keywords: Nb₃Sn, Future Circular Collider, alloying, high field critical current density

1. Introduction

The Future Circular collider (FCC) or upgrades to the Large Hadron Collider (LHC) require Nb₃Sn dipole magnets to operate up to 16 T [1-3], an operating range about twice the Nb-Ti capability of the present LHC magnets [4], and about 5 T higher than the Nb₃Sn magnets planned for the High

Luminosity LHC upgrade [5,6]. To achieve such not yet achieved dipole fields requires magnet conductors with the not yet achieved high current density (J_c) of 1500 A/mm² at 16 T (4.2 K), while simultaneously maintaining high Cu stabilizer residual resistivity ratio (RRR) ≥ 100 and a large strand diameter of order 1 mm [7]. Recent rethinking of the heat

treatment of commercial rod restack process (RRP) conductors has shown that a better optimized Sn mixing heat treatment can allow J_c (16 T, 4.2 K) as high as 1300 A/mm² in specially selected 0.8 mm diameter wires, a significant 20% increase over the best prior standard heat treatment [8]. However, real conductor production has significant spread so there is little hope to achieve FCC specification by this route alone. Powder-In-Tube (PIT) conductor studies indicate generally similar properties to RRP® conductors but with slightly lower performance [9]. The present optimization focus of RRP and PIT commercial conductors is primarily to improve the quality and quantity of the Nb₃Sn in the reaction pack while maintaining high RRR. In summary, there is little expectation that present RRP or PIT conductors can achieve the very challenging 1500 A/mm² at 16 T, 4.2 K FCC specification.

Analysing the challenges emphasizes that high field performance of Nb₃Sn conductors requires minimal loss of upper critical field (H_{c2}) or the more practical irreversibility field (H_{irr}). H_{c2} sets the thermodynamic upper limit of superconductivity: pure binary Nb₃Sn has a H_{c2} of 23.4 T (4.2 K), whereas doping with Group IV (Ti, Hf, Zr) or Group V (Mo, Ta) elements increases the H_{c2} up to ~27 T [10,11]. Ta [12,13] and Ti [14] doping were adopted in PIT and RRP wires and also increase high-field J_c [15]. However, stoichiometry variation across the A15 layer [16,17] and disorder induced by dopants both broaden the H_{c2} distribution [18] and lower H_{irr} [11]. Nb₃Sn conductor optimization involves multiple parameters and understanding of averaged property distributions, reasons why property improvement has somewhat stagnated in recent years. Since there is little sign that H_{c2} can be further enhanced beyond that possible with Ta and/or Ti [11,19], the main issue for the present is clearly to maximize the uniformity of the A15 layer and to avoid any degradation of H_{irr} .

A separate issue is the value of significant enhancement of vortex pinning in the A15 layer. In the general absence of J_c measurements in the 20-25 T range up to H_{irr} , an important indication of enhanced vortex pinning is an upward shift of the field at which the pinning force density F_p ($= |J_c \times \mu_0 H|$) is maximum (H_{Max}), typically 4-5 T. The history of attempts to enhance vortex pinning in Nb₃Sn is quite lengthy. A common theme has been to try to reduce the A15 grain size *and* to introduce additional pinning centres (APCs) into the Nb₃Sn. Ta [20] and Cu [21,22] inclusions were tried without great benefit to J_c , although major effects on enhancing H_{Max} were reported by Rodrigues [22]. The most effective recent results are those observed by irradiation. Transport J_c of 2000 A/mm² at 16 T was achieved in Ti-doped RRP strands after neutron irradiation [19], indicating that point pinning is a route to the FCC specification (though not in a practical conductor fabrication process). The most promising recent results are perhaps those obtained by insulating oxide nanoparticles

created during the reaction heat treatment using a process first developed for a Nb-Zr alloy for a A15 Tape substrate in 1994 at GE [23,24] and also implemented more than a decade ago in experimental filamentary conductors [25-27]. In this route, Zr, originally in dilute solid solution in the Nb, is internally oxidized to insulating ZrO₂ point pins during the A15 reaction heat treatment. Oxygen can be introduced through an easily decomposable oxide such as SnO₂. Such particles increase the pinning force due to a combination of decreased A15 grain size below 50 nm and creation of insulating ZrO₂ point pins [28]. The encouraging results for high field performance are the shift of H_{Max} to higher fields [28,29] and significantly enhanced A15 layer J_c [28,30]. However, H_{irr} of conductors made with binary Nb-Zr alloy was suppressed with respect to clean Nb₃Sn and was far below that of modern Ta/Ti-doped Nb₃Sn [8,14]. Given this H_{irr} degradation, ternary alloys like Nb₄Ta₁Zr are an obvious next step.

This impasse for the FCC conductor motivated the principal questions of this work:

- Is it possible to maintain the high H_{irr} of present commercial Nb₃Sn conductors made with Nb₄Ta/Ti alloys while increasing the pinning site density with ternary alloys based on Nb₄Ta-X (X being Zr or Hf)?
- Does the introduction of oxygen in the system have detrimental effects on the irreversibility field?
- To what extent are A15 grain size refinement and point pinning effects of insulating ZrO₂ or HfO₂ pins individually separable and additive?

In the work reported below we show that Hf is an even more powerful additive to Nb₄Ta than Zr and that an external oxidant is not necessary to greatly enhance vortex pinning. We conclude that the FCC specification is attainable in present commercial Nb₃Sn conductor designs without internal oxygen sources.

2. Experimental methods

We prepared custom alloys with composition Nb₄Ta₁X, using Hf, not just Zr, because they both have high oxygen affinity and can create XO₂ precipitates in the presence of SnO₂. Our Nb₃Sn reaction package is a mixture of Cu-Sn powder surrounding the alloy rod inside a Ta/Cu tube shown in the inset of Figure 5. Monofilaments were made with and without SnO₂ mixed into the Cu-Sn powder. The molar volume ratio of SnO₂ was based on the calculation that 3% of the alloy rod would transform to A15 during heat treatment

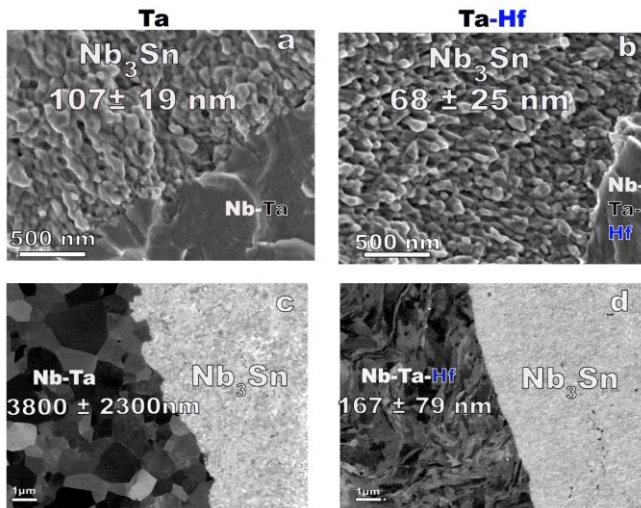


Figure 1. Representative fractographs of the Nb₃Sn/alloy-rod interface in Ta (a,c) and Ta-Hf (b,d) monofilaments after reaction heat treatment at 550°C/100h + 670°C/100h. Significantly smaller Nb₃Sn grain sizes are obtained in the Ta-Hf sample (b) than in the Ta sample (a). Electron channelling contrast in the corresponding Back-Scattered Electron images shows a recrystallized microstructure in the Nb-Ta alloy rod after reaction heat treatment (c) whereas the unreacted Nb-Ta-Hf alloy rod retains a cold worked microstructure.

producing a reaction layer of about 3000-4000 μm². The monofilament wires were drawn down to a final diameter of 2 mm and underwent a two-step heat treatment at 550°C/100h and 670°C/100h. Vibrating-sample magnetometer (VSM) characterizations were performed up to 31 T at the National High Magnetic Field Laboratory to obtain the entire hysteresis loop from which the pinning force and irreversibility fields were calculated. The microstructures were evaluated in a Zeiss 1540 EsB scanning electron microscope (SEM) and a JEOL ARM200cF transmission electron microscope (TEM). Transverse wire cross-sections were prepared by metallographic polishing and then imaged with a solid-state Back-Scattered Electron (BSE) detector, followed by digital image analysis. The TEM specimens were prepared by mechanical polishing on diamond lapping films, followed by Ar ion milling. In the following we will refer to the samples according to the additions with respect to the binary compound (e.g. Ta-Hf is the wire made with Nb₄Ta1Hf alloy, while Ta-Zr-SnO₂ refers to the wire prepared with Nb₄Ta1Zr alloy and SnO₂ powder).

3 Results

3.1 Microstructural characterizations

The in-lens secondary electron (SE) SEM images of fractured wire surfaces of Figure 1(a,b) reveal a typical Nb₃Sn grain structure of the Ta and Ta-Hf wires. The Nb₃Sn grain size of the Ta wire is ~110 nm, comparable to commercial wires. By adding Hf, the A15 grain size noticeably decreases

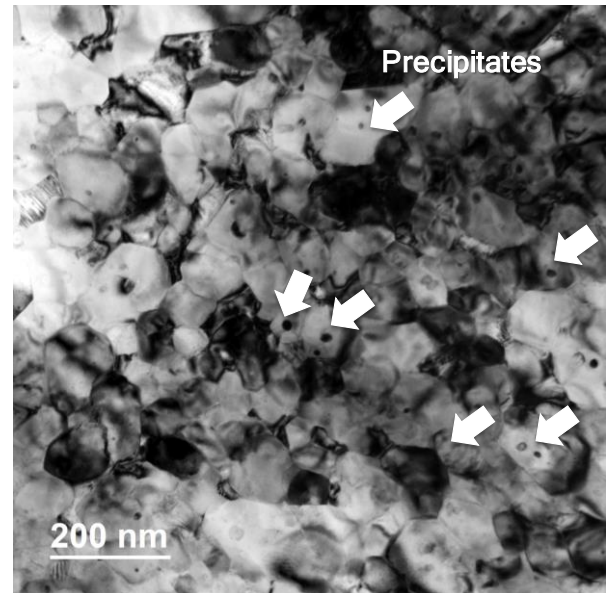


Figure 2. Representative bright field TEM image of Nb₃Sn grains close to the alloy-rod interface. White arrows indicate intragranular precipitates in the Ta-Hf sample reacted at 550°C/100h + 670°C/100h.

to 68±25 nm and 55±10 nm for Ta-Hf and Ta-Hf-SnO₂, respectively. The average grain size for all samples was estimated by the mean lineal intercept method and values are summarized in Table 1.

After the A15 reaction heat treatment, significant Nb alloy rod remains unreacted, leaving a clear microstructural contrast between the alloy rod and the Nb₃Sn as seen in Figure 1(c,d). The channelling contrast in the BSE images highlights evident recrystallization in the Nb₄Ta alloy after the A15 reaction heat treatment (Figure 1(c)), while, in strong contrast, showing that the cold worked deformation structure was retained in the Nb₄Ta1Hf rod (Figure 1 (d)). The grain size of the unreacted rod was 3.8±2.3 μm in the Nb₄Ta but only 0.17±0.08 μm in the Nb₄Ta1Hf rod. For comparison, we also measured the grain size of the unreacted alloy rod in the other alloy samples after the A15 reaction heat treatment at 670°C/100h. The grain size of the unreacted alloy rod was 0.29±0.11 μm and 0.310±0.090 μm in Ta-Zr and Ta-Zr-SnO₂ samples, respectively. Overall the alloys with SnO₂ have slightly smaller grain size than their SnO₂-free counterparts.

Figure 2 shows a TEM bright field image of the Nb₃Sn layer close to the interface with the unreacted Ta-Hf alloy rod, which confirms the very small A15 grain sizes (60-70 nm) of the SEM fractograph of Figure 1 (b). In addition to the A15 diffraction grain contrast, there are also dark dots within the Nb₃Sn grains that correspond to nanoparticle precipitation not visible in the fractograph of Figure 1 (b). No visible precipitates were spotted in the TEM images of the unreacted Nb₄Ta1Hf rod regions. Quantification and chemical analysis

Table 1. Summary of Nb₃Sn properties in monofilament wires prepared with Ta-Zr/Hf-based ternary alloys after a 670°C/100h heat treatment. Results are compared to a 108/127 Ta-doped RRP conductor heat treated at 666°C.

Wire Description			Grain size		Electromagnetic properties at 4.2 K					
Sample Name	Alloy	SnO ₂	Nb ₃ Sn (nm)	Alloy rod μ m	$\mu_0 H_{Max}$ T	$F_{pMax}/F_{pMax}^{Nb-Ta}$	$\mu_0 H_{irr}$ T	Layer $J_c(12T)$ A/mm ²	Layer $J_c(16T)$ A/mm ²	Eq.RRP non-Cu $J_c(16T)$, A/mm ²
Ta	Nb-Ta	No	107±19	3.8±2.3	4.70	1		3210±920	1250±360	750±210
Ta-SnO ₂	Nb-Ta	Yes	100±25	2.6±1.9	5.10	0.65		2240 640	1000±290	600±170
Ta-Zr	Nb-Ta-Zr	No	86±27	0.29±0.11	5.23	1.01	22.8	3550±1010	1280±370	770±220
Ta-Zr-SnO ₂	Nb-Ta-Zr	Yes	70±33	0.31±0.09	5.30	1.54	20.9	5020±1430	1680±480	1010±290
Ta-Hf	Nb-Ta-Hf	No	68±25	0.17±0.08	5.81	2.35	23.6	9610±2740	3710±1060	2230±640
Ta-Hf-SnO ₂	Nb-Ta-Hf	Yes	55±10	0.13±0.06	5.47	2.25	23.1	8520±2430	3090±880	1860±530
Ta-RRP	Nb-Ta	-			4.60					23.2

of the precipitates are in progress. Preliminary Electron Energy Loss Spectroscopy (EELS) indicated that the precipitates are Sn deficient without detectable oxygen.

Since the Nb₃Sn layers formed by Sn diffusion develop compositional and/or microstructural gradients away from the Sn source, we also examined the Nb₃Sn layer close to the Cu-Sn region, confirming that the Sn-rich Nb₆Sn₅ phase was also produced in this rod-in-powder-in-tube design. Figure 3 is a TEM image of the interface between the outer Nb₆Sn₅ and the inner Nb₃Sn layer (the unreacted Nb₄Ta₁Hf rod lies inside these layers). An interesting observation is the presence of very small equiaxed Nb₆Sn₅ grains of less than 100 nm diameter. This is one of the first observations of sub-micron Nb₆Sn₅, whose grain size is normally several microns in commercial PIT conductors [13].

3.2 Magnetization characterizations

Magnetization measurements were performed in the 1.3-14 K temperature range on all the monofilament wires and, for comparison, a Ta-doped RRP® conductor which was

similarly heat treated (666°C/50h). The 35 T magnet allowed us to evaluate the entire hysteresis loops so as to accurately estimate the temperature dependence of H_{irr} . The layer J_c and F_p were estimated using the Bean model combined with the cross-sectional dimensions determined by SEM image analysis. The A15 Thickness and area fraction was identified based on BSE contrast differences. Because of the simple wire design and some non-uniform deformation of the Nb alloy rods during wire drawing, a noticeable variation in the residual rod cross-section was found within each wire, affecting the calculation of Nb₃Sn cross-sectional area. To estimate the layer J_c , we analysed 10 different wire cross-sections to determine the average rod and Nb₃Sn cross-sectional areas and their respective standard deviations.

The deduced layer F_p and J_c values are plotted in Fig. 4 and in the inset of Fig. 6. For the standard Nb₄Ta alloy (without SnO₂) F_p peaks at $H_{Max} \sim 4.7$ T, close to the value for Ta-doped RRP® wire (see Table 1). Adding SnO₂ to the Ta-doped wire shifts H_{Max} above 5 T but clearly suppresses F_{pMax} by 35%. The Nb₄Ta₁Zr alloy shifts H_{Max} to ~ 5.2 -5.3 T with F_{pMax} for the wire without SnO₂ being comparable to that of the standard Nb₄Ta alloy, whereas the wire with SnO₂ addition has a more than 50% larger F_{pMax} . These two curves however cross at high field due to some H_{irr} degradation when SnO₂ is present. The

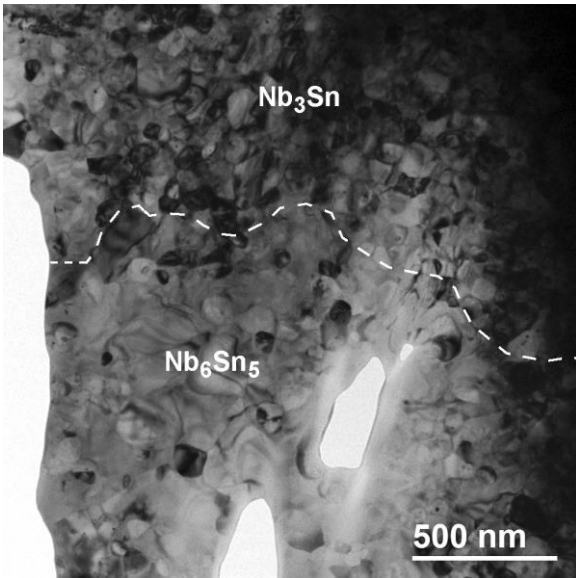


Figure 3. Representative TEM bright field image of the Nb₃Sn-Nb₆Sn₅ interface in the Ta-Hf sample reacted at 550°C/100h + 670°C/100h. Grain sizes of both Nb₆Sn₅ and Nb₃Sn are below 100 nm.

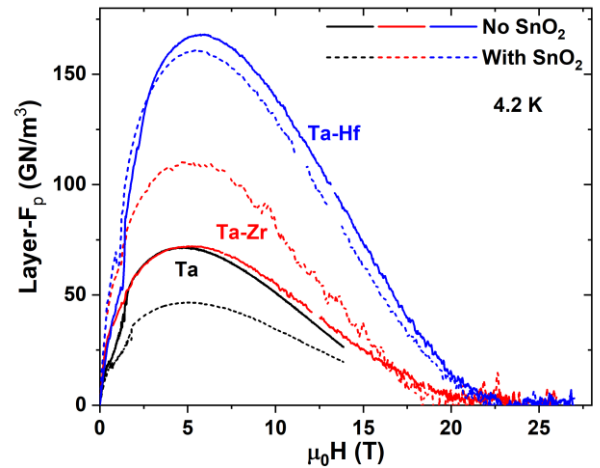


Figure 4. Pinning force density of the A15 layer as a function of magnetic field showing significant enhancement for the Nb-Ta-Zr and Nb-Ta-Hf conductors.

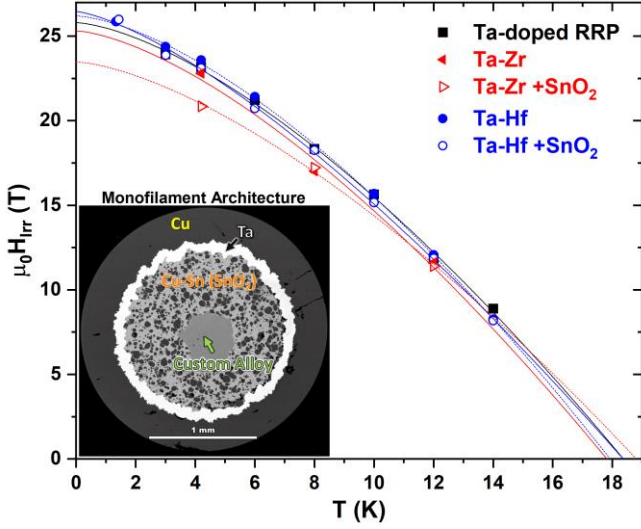


Figure 5. Irreversibility field versus temperature determined from the magnetization hysteresis of the various monofilaments compared with a Ta-doped RRP conductor. H_{irr} of the Ta-Hf doped monofilament is the highest and both Zr and Hf monofilaments with SnO_2 show degraded H_{irr} . The inset shows an unreacted monofilament cross-section.

$\text{Nb}_4\text{Ta}_1\text{Hf}$ alloy is clearly the most effective in changing the pinning force, having H_{Max} peaking at ~ 5.5 and ~ 5.8 T for the wires with and without SnO_2 , respectively. F_{pMax} values in these cases are comparable and both more than 2.2 times larger than for the standard Nb_4Ta alloy.

The temperature dependence of H_{irr} is shown in Fig. 5. Comparing the 4.2 K values, we found that Ta-Zr, and Ta-Hf without SnO_2 have H_{irr} values of 22.8 and 23.6 T, respectively, similar to H_{irr} of 23.2 T obtained for the RRP conductor. The SnO_2 addition to the Ta-Zr sample suppresses $H_{irr}(4.2\text{ K})$ to 20.9 T, whereas in the Ta-Hf case H_{irr} had a smaller drop from 23.6 to 23.1 T. Overall, oxygen appears to degrade both Hf and Zr-doped conductors but the effect is larger for the $\text{Nb}_4\text{Ta}_1\text{Zr}$ alloy.

Figure 6 and Table 1 summarize the layer $J_c(4.2\text{ K})$ at 12 and 16 T of our monofilaments and compare them to commercial conductors: the grey shaded areas represent the range of variation for high- J_c Ta-doped RRP® from ref. 31, while the orange dashed lines are for the best Ti-doped RRP® after the optimized Cu-Sn mixing heat treatment of ref. 8. Our Nb_4Ta wire has a layer J_c of $3210 \pm 920\text{ A/mm}^2$ at 12 T and $1250 \pm 360\text{ A/mm}^2$ at 16 T, values typical of those found for Ta-doped RRP® conductors, which range between 3190-5250 A/mm^2 at 12 T and 1400-1880 A/mm^2 at 16 T. The Ti-doped RRP® conductor after optimized heat treatment has markedly better 16 T properties, with a layer $J_c > 2000\text{ A/mm}^2$. Oxygen addition to the Nb_4Ta monofilament reduces the layer J_c below the oxygen-free Nb_4Ta values ($2200 \pm 640\text{ A/mm}^2$ at 12 T and $1000 \pm 290\text{ A/mm}^2$ at 16 T). Additions of 1Zr to Nb_4Ta improve the layer J_c of the conductor to $3550 \pm 1010\text{ A/mm}^2$ (12 T) and $1280 \pm$

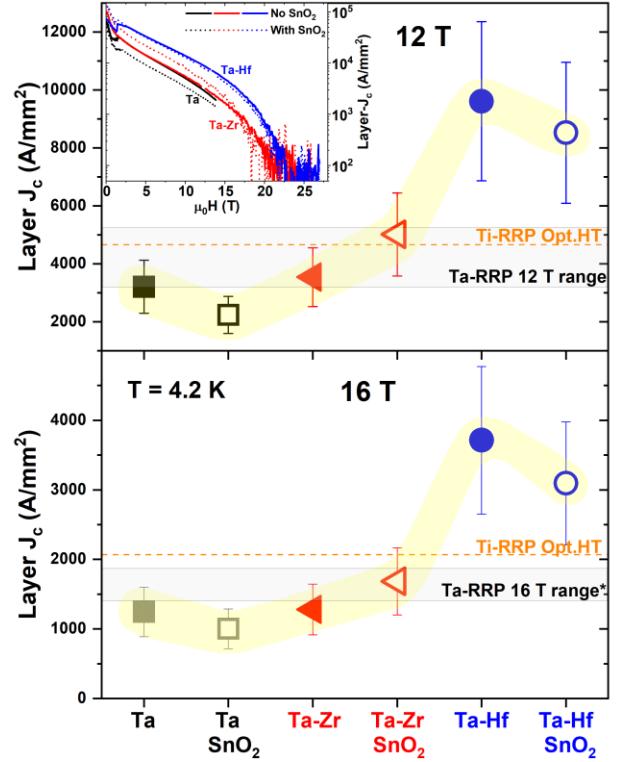


Figure 6. Layer $J_c(4.2\text{ K})$ of Nb_3Sn in monofilament wires at 12 and 16 T (4.2 K) showing significantly better performance in the Ta-Hf based conductors with respect to the standard Ta and Ta-Zr based wires by about a factor of three. The grey shaded areas represent the range of variation for high- J_c Ta-doped RRP® [31]; the orange dashed lines are for the best Ti-doped RRP® wire after optimized heat treatment [8]. The 16 T data for the Ta and Ta- SnO_2 samples and the Ta-RRP conductors were estimated from 14 T measurements.

370 A/mm^2 (16 T), and oxygen addition further improves the layer J_c to 5020 A/mm^2 at 12 T and 1680 A/mm^2 at 16 T. However, the most interesting results are obtained in the $\text{Nb}_4\text{Ta}_1\text{Hf}$ monofilaments where the layer J_c without SnO_2 is well above all other conductors, exceeding 9600 A/mm^2 at 12 T and $3710 \pm 1060\text{ A/mm}^2$ at 16 T. Unlike its $\text{Nb}_4\text{Ta}_1\text{Zr}$ counterpart, the Hf conductor shows a slight layer- J_c decrease with oxygen addition. However, the values are still very high (8520 A/mm^2 at 12 T and 3090 A/mm^2 at 16 T).

4. Discussion

Despite the observation of an upward shift in F_{pMax} towards higher field, earlier Nb_1Zr PIT conductors showed degraded H_{irr} of ~ 20 T or less, lower than binary Nb_3Sn , thus depressing the high field J_c properties significantly below standard Ta or Ti-doped conductors [8,14]. A new result of this work is that H_{irr} suppression is no longer an issue for conductors fabricated with Nb_4Ta alloy with 1Zr or 1Hf additions. The A15 $H_{irr}(4.2\text{ K})$ now reaches 23.6 T in the O-free Hf alloy without any degradation compared to commercial wires made with Nb_4Ta and Nb-Ti. The beneficial effects of Zr added to

Nb4Ta in a PIT wire have also been recently reported by Xu *et al.* [32]. However, in this comparison of properties with and without SnO₂, we note that we do still see a small H_{irr} degradation in the presence of O, the effect being significantly worse in the Zr alloy. Although showing an improved H_{Max} of 5.3 T, the Nb4Ta1Zr alloy with SnO₂ has H_{irr} (4.2 K) of only 20.85 T, ~2 T lower than Nb4Ta1Zr without SnO₂.

Perhaps the most surprising result of the present study is that the Nb₃Sn grain size can be reduced to much less than 100 nm without SnO₂ and its internal oxidation potential when Nb4Ta1Hf alloy is used, perhaps because some nano-precipitates form in the A15 layer even without internal oxidation by SnO₂. The explanation may lie in another unexpected observation, namely that neither the Nb4Ta1Zr nor the Nb4Ta1Hf alloys recrystallized during the A15 reaction heat treatment, quite unlike the case with Nb4Ta (or pure Nb) rods. As seen in Figure 1 and Table 1, the grain structure of the Nb4Ta1Zr and Nb4Ta1Hf rods after A15 reaction heat treatment is one order of magnitude smaller than in the recrystallized Nb4Ta alloy. Since penetration of Sn into the alloy must occur preferentially by grain boundary diffusion [33], the much denser diffusion paths available to the unrecrystallized ternary alloys must contribute significantly to denser A15 nucleation and a finer A15 grain size in the growing reaction layer. Indeed we propose that a high A15 nucleation frequency in the cold-worked alloy nanostructure with its high GB density is the dominant factor to significantly reduce the Nb₃Sn grain size in our Ta-Zr and Ta-Hf samples. Our observation of 100 nm grains in the intermediate Nb₆Sn₅ phase which forms between the Sn source and the A15 layer is also consistent with this same Sn diffusion mechanism along the Nb alloy GBs. SnO₂ addition does appear to produce a small decrease in A15 grain size (from 68 to 55 nm), perhaps by providing some precipitation that retards A15 grain growth. In this respect the 1Hf alloy appears better than the 1Zr alloy precisely because it can strongly enhance vortex pinning without need for SnO₂ and without the H_{irr} degradation that O brings in these wires.

In considering the practical implications of these experiments, we note that the highest non-Cu J_c (4.2 K, 16 T) obtained by optimized heat treatment of state-of-the-art commercial Ti-doped RP® conductor is so far only ~1300 A/mm². This new record for an RRP conductor emerged from a detailed study of a wide range of RRP billets made available through the US Magnet Development Program and Oxford Superconducting for study by Sanabria *et al.*[8], most of which were of lower J_c due to the inherent distribution of properties seen in large production runs. The present results have a particular excitement that the highest J_c was obtained in the Nb4Ta1Hf alloy without SnO₂, suggesting that conventional RRP® or PIT architectures are possible with minimum perturbation to present billet designs. The RRP® version might thus create <100 nm Nb₃Sn grains with a layer

J_c (4.2 K, 16 T) of ~3700 A/mm². Considering that the Nb₃Sn layer occupies about 60% of the non-Cu area in RRP® wires, this is equivalent to a non-Cu J_c (4.2 K, 16 T) of ~2200 A/mm², well above the FCC requirement of 1500 A/mm². Moreover, the Nb1Ta4Hf alloy could also be beneficial for PIT conductors presently made with Nb4Ta tubes. Detailed studies of the A15 reaction in present PIT conductors by Segal *et al.* show that J_c is in fact limited by the fact that about one quarter of the ~55% A15 (formed by decomposition of large grain Nb₆Sn₅) is >1 μm in size [12,13,34]. This large grain A15 does not contribute to current transport, thus degrading the overall J_c of PIT conductors with respect to RRP® conductors. Segal's studies showed that the large grain A15 could be partially suppressed in favour of fine-grain A15 at higher reaction temperatures. J_c did not benefit however due to the larger A15 grain size of higher temperature reactions, presumably associated with grain growth in the recrystallized Nb4Ta. Given the ability of Nb4Ta1Hf to avoid recrystallization, it may be that the inverted higher-lower temperature A15 reactions studied by Segal now become feasible.

In summary we have shown that 1Hf additions to Nb4Ta show many benefits and suggest straightforward routes to much higher J_c Nb₃Sn conductors made by all of the present commercial routes, bronze, internal Sn and other variants. A potential concern may be that both Zr and Hf additions to Nb4Ta degrade alloy drawability, but, so far, after a true strain of 8, no problems of work hardening and filament breakage have been encountered. Further studies to higher strains are in progress.

5. Conclusions

We have demonstrated that adding 1Hf or 1Zr to Nb4Ta greatly reduces the H_{irr} suppression encountered in Nb₃Sn wires made from Nb1Zr wires previously examined at OSU and SupraMagnetics/FSU [28-30]. The highest H_{irr} and the best vortex pinning performance were obtained with a Nb4Ta1Hf alloy without SnO₂, which reached a maximum pinning force more than twice that obtained with standard Nb4Ta alloy and with slightly better H_{irr} . Initial evaluations of the layer J_c lead to $\sim 3700 \pm 1100$ A/mm² at 16 T, 4.2 K corresponding to a non-Cu J_c of $\sim 2200 \pm 600$ A/mm² in an RRP architecture. These results indicate that the quickest pathway to a high J_c for FCC conductor may be to avoid internal oxidation and to just use the A15 grain refinement properties of Hf or similar additions to Nb4Ta in either internal-tin or PIT conductors.

Acknowledgements

The authors would like to thank to J. Parrell (Bruker OST, LLC) for providing Nb7.5 Ta slabs used for the special alloys melted here and Eun Sang Choi (NHMFL) for his support during high-field VSM characterization. The authors would

like to acknowledge the TEM sample preparation work of undergraduate students T. Shelby and J. Boyd (NHMFL-ASC). Discussions with Chris Segal (now at CERN) are gratefully acknowledged. This work is funded by the U.S. Department of Energy, Office of Science, and Office of High Energy Physics under Award Number DE-SC0012083, and performed under the purview of the US-Magnet Development Program. Discussions of parallel work being performed by Xingchen Xu (Fermilab) are greatly acknowledged. This work

was performed at the National High Magnetic Field Laboratory, which is supported by National Science Foundation Cooperative Agreements NSF-DMR-1157490 and DMR-1644779 and by the State of Florida.

References

- [1] Todesco E *et al* 2018 Progress on HL-LHC Nb₃Sn Magnets *IEEE Trans. Appl. Supercond.* **28** 1–9
- [2] Tommasini, D *et al* 2018 Status of the 16 T Dipole Development Program for a Future Hadron Collider *IEEE Trans. Appl. Supercond.* **28** 1–5
- [3] Schoerling D *et al* 2017 Considerations on a Cost Model for High-Field Dipole Arc Magnets for FCC *IEEE Trans. Appl. Supercond.* **27** 1–5
- [4] Bottura L, de Rijk G, Rossi L and Todesco E 2012 Advanced Accelerator Magnets for Upgrading the LHC *IEEE Trans. Appl. Supercond.* **22** 4002008–4002008
- [5] Pan H *et al* 2016 Assembly Tests of the First Nb₃Sn Low-Beta Quadrupole Short Model for the Hi-Lumi LHC *IEEE Trans. Appl. Supercond.* **26** 4001705
- [6] Savary F *et al* 2017 Progress on the Development of the Nb₃Sn 11T Dipole for the High Luminosity Upgrade of LHC *IEEE Trans. Appl. Supercond.* **27** 4003505
- [7] Tommasini D *et al* 2017 The 16 T Dipole Development Program for FCC *IEEE Trans. Appl. Supercond.* **27** 4000405
- [8] Sanabria C *et al* Controlling Cu–Sn mixing so as to enable higher critical current densities in RRP @ Nb₃Sn wires *Supercond. Sci. Technol.* **31**, 064001 (2018).
- [9] Bordini B *et al.* The Bundle-Barrier PIT Wire Developed for the HiLumi LHC Project *IEEE Trans. Appl. Supercond.* **27**, 6000706 (2017).
- [10] Suenaga M 1985 Optimization of Nb₃Sn *IEEE Trans. Magn.* **21** 1122–1128
- [11] Suenaga M, Welch D O, Sabatini R L, Kammerer O F and Okuda S. 1986 Superconducting critical temperatures, critical magnetic fields, lattice parameters, and chemical compositions of “bulk” pure and alloyed Nb₃Sn produced by the bronze process *J. Appl. Phys.* **59** 840–853
- [12] Tarantini C *et al* 2015 Composition and connectivity variability of the A15 phase in PIT Nb₃Sn wires *Supercond. Sci. Technol.* **28** 095001
- [13] Segal C *et al* 2016 Evaluation of critical current density and residual resistance ratio limits in powder in tube Nb₃Sn conductors *Supercond. Sci. Technol.* **29** 085003
- [14] Tarantini C, Sung Z H, Lee P J, Ghosh A K and Larbalestier D C 2016 Significant enhancement of compositional and superconducting homogeneity in Ti rather than Ta-doped Nb₃Sn *Appl. Phys. Lett.* **108** 042603
- [15] Field M B, Zhang Y, Miao H, Gerace M and Parrell J A 2014 Optimizing Nb₃Sn Conductors for High Field Applications *IEEE Trans. Appl. Supercond.* **24** 1–5
- [16] Godeke A *et al* 2005 The upper critical field of filamentary Nb₃Sn conductors *J. Appl. Phys.* **97** 093909
- [17] Fischer C M, Lee P J and Larbalestier D C 2002 Irreversibility field and critical current density as a function of heat treatment time and temperature for a pure niobium powder-in-tube Nb₃Sn conductor *AIP Conf. Proc.* **614** 1008–1015
- [18] Heald S M *et al* 2018 Evidence from EXAFS for Different Ta/Ti Site Occupancy in High Critical Current Density Nb₃Sn Superconductor Wires. *Sci. Rep.* **8** 4798
- [19] Baumgartner T *et al* 2015 Performance Boost in Industrial Multifilamentary Nb₃Sn Wires due to Radiation Induced Pinning Centers. *Sci. Rep.* **5** 10236
- [20] Klemm M, Seibt E, Specking W, Xu J Q and Flukiger E 1990 *Supercond. Sci. Technol.* **3** 249
- [21] Zhou B R, Hong S and Kear B H 1994 Improver pinning in Nb and Nb₃Sn superconductors *Philos. Mag. B* **71** 427–436
- [22] Rodrigues C A and Rodrigues D J 2007 Flux Pinning Behavior of Nb₃Sn Superconductors With Nanostructured Pinning Centers *IEEE Trans. Appl. Supercond.* **17** 2627–2630
- [23] Rumaner L E and Benz M G Effect of oxygen and zirconium on the growth and superconducting properties of Nb₃Sn *Metall. Mater. Trans. A* **25** 203–212
- [24] Rumaner L E, Benz M G and Hall E L 1994 The role of oxygen and zirconium in the formation and growth of Nb₃Sn grains *Metall. Mater. Trans. A* **25** 213–219
- [25] Zeitlin B A, Marte J S, Ellis D, Benz M and Gregory E 2004 Some Effects of the Addition of 1 At. % Zr to Nb on the Properties and Ease of Manufacture of Internal- Tin Nb₃Sn *AIP Conf. Proc.* **711** 395–402
- [26] Zeitlin B A *et al* 2005 Results on mono element internal tin Nb₃Sn conductors (MEIT) with Nb7.5 Ta and Nb(1Zr+O_x) filaments. *IEEE Trans. Appl. Supercond.* **15** 3393–3398
- [27] Zeitlin B A *et al* 2006 The Effect on the Superconducting Properties of the Addition of Oxygen and Titanium to (Nb- 1Zr)₃Sn Mono Element Internal Tin (MEIT) Conductors. *AIP Conf. Proc.* **824** 513–519
- [28] Xu X, Sumption M, Peng X and Collings E W 2014 Refinement of Nb₃Sn grain size by the generation of ZrO₂ precipitates in Nb₃Sn wires. *Appl. Phys. Lett.* **104** 082602
- [29] Motowidlo L R *et al.* 2018 An intermetallic powder-in-tube approach to increased flux-pinning in Nb₃Sn by internal oxidation of Zr. *Supercond. Sci. Technol.* **31** 014002
- [30] Xu X, Sumption M D and Peng X 2015 Internally Oxidized Nb₃Sn Strands with Fine Grain Size and High Critical Current Density. *Adv. Mater.* **27** 1346–1350
- [31] Tarantini C *et al* 2014 Examination of the trade-off between intrinsic and extrinsic properties in the optimization of a modern internal tin Nb₃Sn conductor *Supercond. Sci. Technol.* **27** 065013
- [32] Xu X *et al.*, private communication.
- [33] Smathers D B 1982 Ph.D Thesis, University of Wisconsin Madison
- [34] Segal C *et al* Improvement of small to large grain A15 ratio in Nb₃Sn PIT wires by inverted multistage heat treatments 2017 *IOP Conf. Ser.: Mater. Sci. Eng.* **279** 012019